Compact and Tunable Microstrip Bandpass Filter Using a Disk Resonator and a U-shaped Waveguide for Wi-MAX and WLAN Applications

Shiva Khani[1*]

***Abstract*— In this paper, a microstrip dual-band bandpass filter containing a disk resonator and a U-shaped waveguide is designed. The proposed structure generates two pass-bands with resonance frequencies of 3.7 and 5.7 GHz which can be used for Wi-MAX and WLAN applications, respectively. It is worth mentioning that two resonance frequencies are located in a relatively wide frequency range of 0 to 10 GHz. The simulation results show that the insertion losses and return losses of two pass-bands are better than 0.62, 0.75 dB, and 21.9, 20.1 dB, respectively. Furthermore, its total size is equal to 12.9×9.5 mm^2. In addition to the simple structure of the proposed filter, its second resonance frequency can be tuned by changing only the radius of the disk resonator, without the need to change the overall structure or add another element to the filter structure. Furthermore, this filter's symmetrical structure has caused no distinction between the input and output ports, which facilitates the mass production of this structure. The other remarkable features of the suggested filter are its compact size, low insertion loss, high return loss, sharp transition bands, high attenuation level in the stop-bands, wide upper stop-band bandwidth, and sharpness of transient bands.**

***Index Terms*— Microstrip bandpass filter, Disk resonator, U-shaped waveguide, Tunable frequency, Compact size.**

I. INTRODUCTION

Microstrip structure is a kind of electrical transmission line that is used to convey microwave frequency signals. It consists of three layers, including a strip conductor layer on a dielectric substrate supported by a ground plane [1]. Due to the importance and widespread application of such topologies (metal insulator metal topologies), they are also used today in terahertz applications such as metal insulator metal plasmonic structures [2-5]. Such devices include plasmonic filters [6-10], absorbers [11-13], splitters [14-16], sensors [17-19], logic gates [20-22], modulators [23-25], switches [26-28], brag reflectors [29, 30], demultiplexes [31-33], and so on.

It is worth mentioning that all devices mentioned above can be redesigned in microwave frequencies using microstrip structures [34-39]. Microstrip filters are widely used in various microwave communication systems. [40]. Among microstrip filters, bandpass (BP) filters [41, 42] and low-pass filters [43] are of high importance and will be discussed in this paper. In recent years, various structures and resonator shapes have been used to reach high-performance microstrip BP filters.

Having remarkable advantages, disk resonators are among the common types of resonators that can be used to design microstrip filters [44, 45]. For example, by varying its radius, the resonance frequency can be tuned, and it is also easy to fabricate. Furthermore, it typically has a more compact size compared to other resonator shapes. Another resonator structure that has been used to improve the BP microstrip filter design features is the stepped impedance resonator [46, 47]. While this resonator can achieve a broad stopband bandwidth and high levels of attenuation in the stopbands, it is large and produces gradual transient bands.

Ring resonators [48] as another structure have been proposed in a diversity of various forms of circular [49], square [50], hexagonal [51], and rectangular [52] ring resonator systems. Moreover, there are other resonator structures such as T-shaped resonators [53], U-shaped resonators [14], tapered resonators [54], spiral-shaped resonators [55], etc. to design microstrip BP filters. It is worth mentioning that filters can be used as basic structures to design and fabricate other devices such as antennas [56, 57], power dividers [58, 59], diplexers [60, 61], oscillators [62], and so on. As a result, the design, analysis, and fabrication of filters are among the important topics in today's research.

In this paper, a simple, symmetrical, and interesting configuration is achieved by utilizing a disk resonator coupled to a U-shaped waveguide through a stub resonator. On the other hand, its second resonance frequency can be easily adjusted without increasing the overall size. In addition to the mentioned features, it has other suitable parameters such as compact size, low insertion loss and high return loss at resonance frequencies, high attenuation level in the stop-bands, wide upper stop-band bandwidth, and sharpness of transient bands.

This paper is organized as follows: section II introduces the microstrip BP filter designed in the study along with its frequency response. Section III discusses the initial filter structure (Filter I) and compares it with the proposed filter (Filter II). In section IV, the effect of structural parameters on the frequency response of the proposed filter is investigated. Also, the tunability of the filter is shown in this section. Section V discusses the surface current distribution of the proposed

1. Faculty of Electrical and Computer Engineering, Semnan University, Semnan, Iran.

Corresponding author Email: shiva.khani@semnan.ac.ir

filter. The two last sections are devoted to performance comparisons of the proposed filter with other similar works and conclusions, respectively.

II. DUAL-BAND BP FILTER DESIGN AND RESULTS

Fig. 1 shows the schematic view of the microstrip dual-band BP filter designed in this paper. As seen in this figure, this structure is composed of a disk resonator and a U-shaped waveguide. The disk resonator is coupled to the waveguide through a stub resonator. Furthermore, input and output ports are coupled to the waveguide through inverted U-shaped structures. The structural parameters shown in Fig. 1 are as follows: r_1= 1.5, r_2= 5, r_3= 6, l_1= 0.85, l_2= 3, l_3= 3.794, w_1= 0.75, w_2= 1.95, w_3= 1.4, g_1= 0.3, g_2= 0.15 (all in mm).

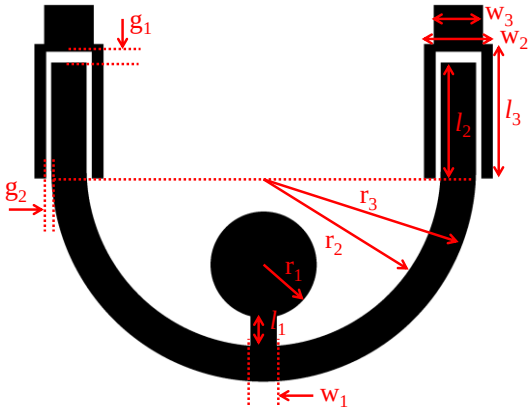

Fig. 1. Schematic view of the proposed dual-band BP filter.

The S-parameters of the proposed BP filter are shown in Fig. 2. This figure shows that the proposed filter generates two narrow passbands at the center frequencies of 3.7 and 5.7 GHz in an almost wide frequency range of 0 to 10 GHz. The EM simulation results show that the insertion losses of the first and second bands are 0.62 and 0.75 dB, respectively. Moreover, their return losses are equal to 21.9 and 20.1 dB, respectively. Also, as seen, the attenuation level throughout the stopbands (before the first resonance frequency, between two resonance frequencies, and after the second resonance frequency) is less than -20 dB. Therefore, this attenuation level can guarantee that almost no frequency passes through the filter in these bands.

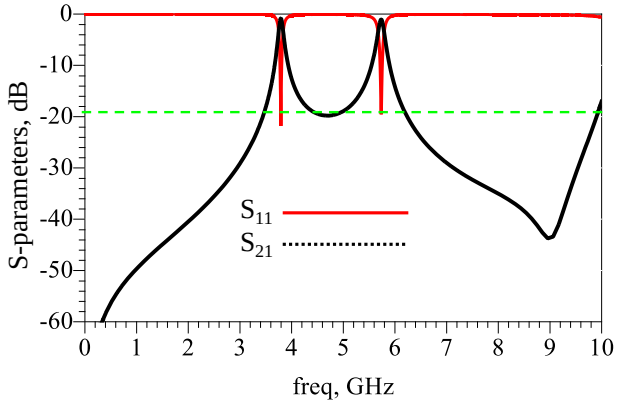

Fig. 2. Frequency response of the proposed dual-band BP filter.

III. INITIAL FILTER STRUCTURE

In this section, to provide a better view of the design procedure of the proposed structure, the initial filter designed in this paper (Filter 1) is studied and compared to the main filter (Filter 2). Fig. 3 shows the schematic view of Filter 1 and Filter 2 and their frequency responses. As seen in this figure, the only difference between Filter 1 and Filter 2 structures is the shape of the waveguide, which is a straight-shaped waveguide for Filter 1. The length of L in Fig. 3(a) is 25 mm. The values of other parameters remain unchanged.

By bending the straight-shaped waveguide in Filter 1 and turning it into a U-shaped waveguide in Filter 2, not only the total length of the filter is reduced but also the frequency response is improved. For example, the resonance frequencies shift to higher frequencies (desirable frequencies). As known, frequency and wavelength are inversely proportional to each other. In other words, the higher the frequency, the shorter the wavelength. For example, microwave devices [63, 64] that work in the GHz frequency range have dimensions of millimeters, while optical devices [65, 66] that work in the terahertz range have dimensions of nanometers. Therefore, in this design as well, as the dimensions of the filter become more compact, the operating wavelength of the device shifts to lower wavelengths, or in other words, the working frequency of the device shifts to higher frequencies.

Also, insertion losses and return losses in both passbands improve. It is worth mentioning that the insertion losses and return losses of the first and second bands for Filter 1 are 1.07, 1.21dB, and 18.9, 19.03 dB, respectively. Furthermore, the stopband bandwidth expands to about 10 GHz.

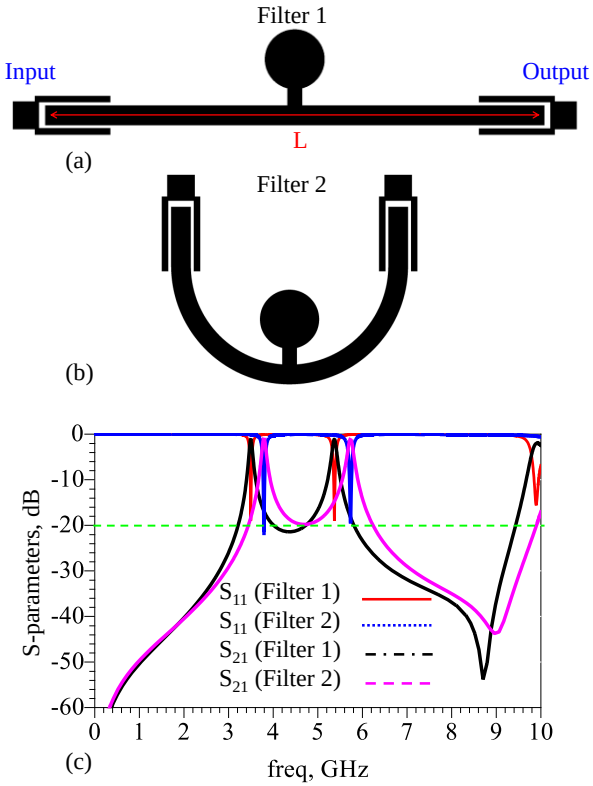

Fig. 3. (a) Schematic view of the initial filter (Filter I), (b) Schematic view of the proposed filter (Filter II), (c) Frequency responses of Filter I and Filter II.

It is worth mentioning that in addition to the mentioned method for compressing the filter proposed in this paper (U-shaped waveguide), some other methods are suggested in other publications. For example, a meander waveguide [67], a spiral resonator [68], and coupled hairpin resonators [69], are used to compress the filter structures. Although all such methods reduce the total size of the filters, they have a complex and difficult fabrication process. The approach presented in this paper stands out due to its straightforward design, effectively eliminating the drawbacks discussed earlier.

IV. INVESTIGATION OF THE STRUCTURAL PARAMETERS' EFFECTS AND TUNABILITY OF THE PROPOSED FILTER

After detailing the proposed filter and its design methodology, its structural parameters are swept to investigate their effects on the frequency response. First, the gap of g_1 is changed from 0.2 to 0.4 mm with the steps of 0.05 mm while the values for the other structural parameters have been assumed to be constant. Fig. 4 shows this modification. As seen in this figure, when the g_1 value increases, the magnitudes of S_{21} and S_{11} have no changes in the frequency range of 0 to 10 GHz.

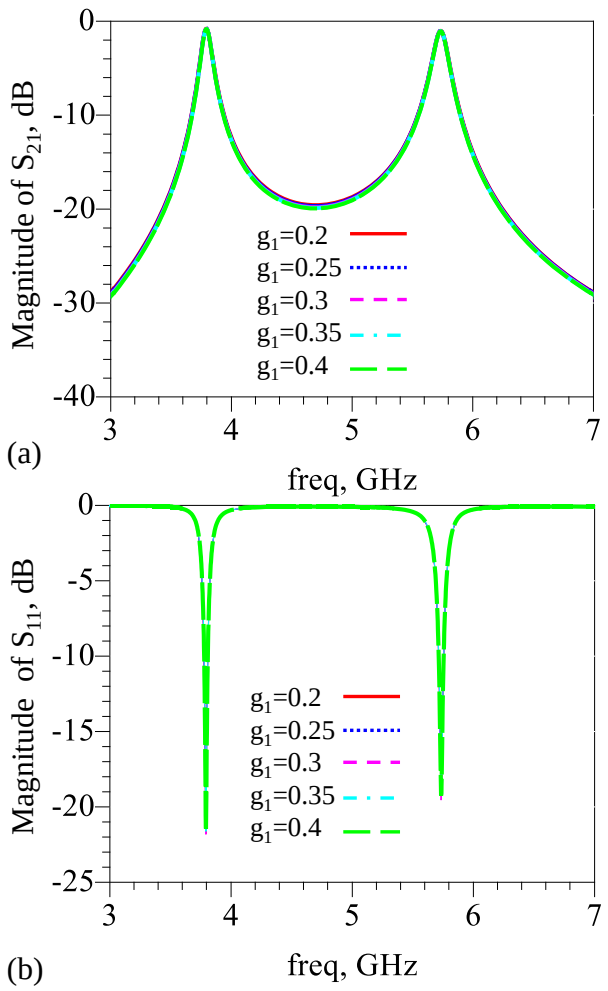

Fig. 4. Frequency response of the proposed dual-band BP filter for different values of g_1 (a) S_{21}, (b) S_{11}.

Since low values for g_1 complicate the fabrication process and high values for g_1 increase the total dimensions of the structure, the value of g_1= 0.3 mm, as a middle value, is considered for this parameter.

Fig. 5 shows the changes in the other parameter (g_2). By increasing the g_2 value, return loss values at stopbands and bandwidths of two passbands decrease. This is because increasing the g_2 value decreases the coupling strength between the waveguide and inverted U-shaped structures. Although the values of g_2> 0.15 mm provide better return losses for stopbands, they also lead to a narrower bandwidth for the passbands, which needs more precision for the fabrication process. On the other hand, the values of g_2< 0.15 mm also make the fabrication process difficult. Therefore, the best value for g_2 is 0.15 mm.

The next structural parameters are the width and length of the stub resonator (w_1 and l_1). Figs. 6 and 7 show that by increasing the w_1 value and decreasing the l_1 value separately, the first resonance frequency does not change and the second resonance frequency has a little shift towards higher frequencies. Therefore, for both modes, values are chosen for which the second resonance frequency is located in the desired place. These values are w_1= 0.75 and l_1= 0.85 mm.

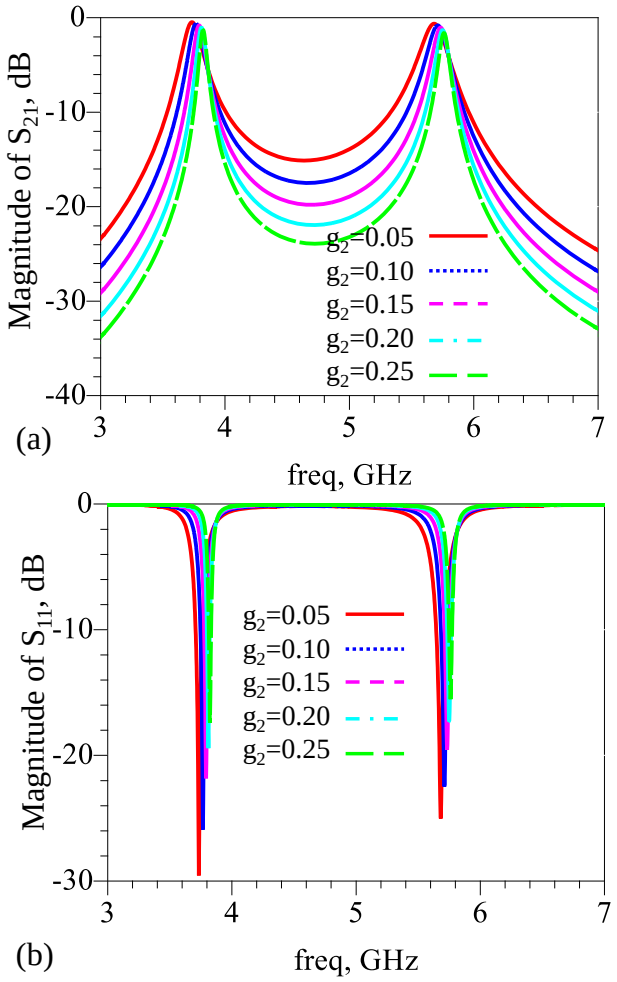

Fig. 5. Frequency response of the proposed dual-band BP filter for different values of g_2 (a) S_{21}, (b) S_{11}.

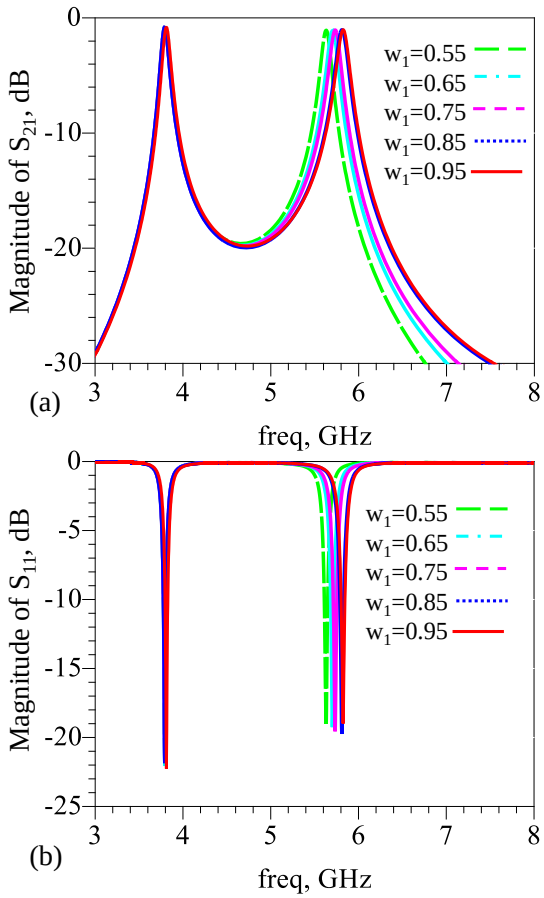

Fig. 6. Frequency response of the proposed dual-band BP filter for different values of w_1 (a) S_{21}, (b) S_{11}.

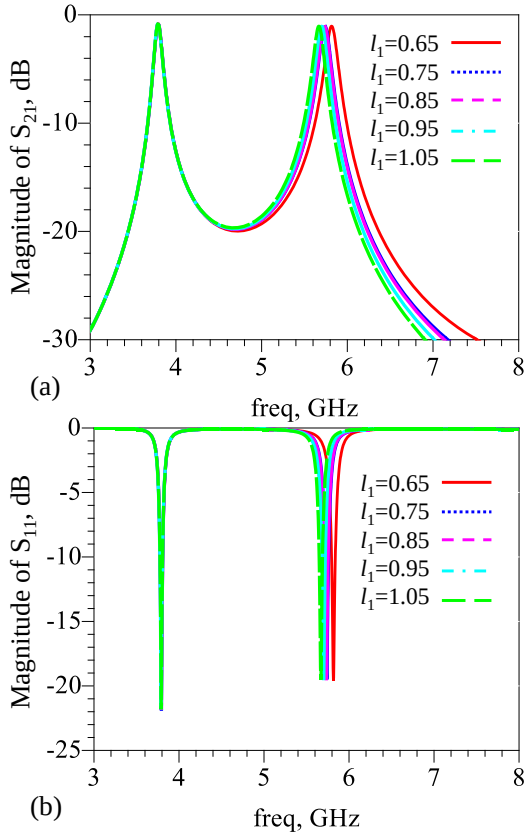

Fig. 7. Frequency response of the proposed dual-band BP filter for different values of l_1 (a) S_{21}, (b) S_{11}.

The last structural parameter is the radius of the disk resonator (r_1). As shown in Fig. 8, by increasing the r_1 value from 1.3 to 1.7 mm with the steps of 0.1 mm, the location of the second resonance frequency shifts to lower frequencies, while the first resonance frequency remains unchanged. Given the wide range of changes in the second frequency location, it can be concluded that the proposed filter is tunable at the second band without alteringthe total size of the circuit. This property is one of the notable features of the BP filter designed in this paper.

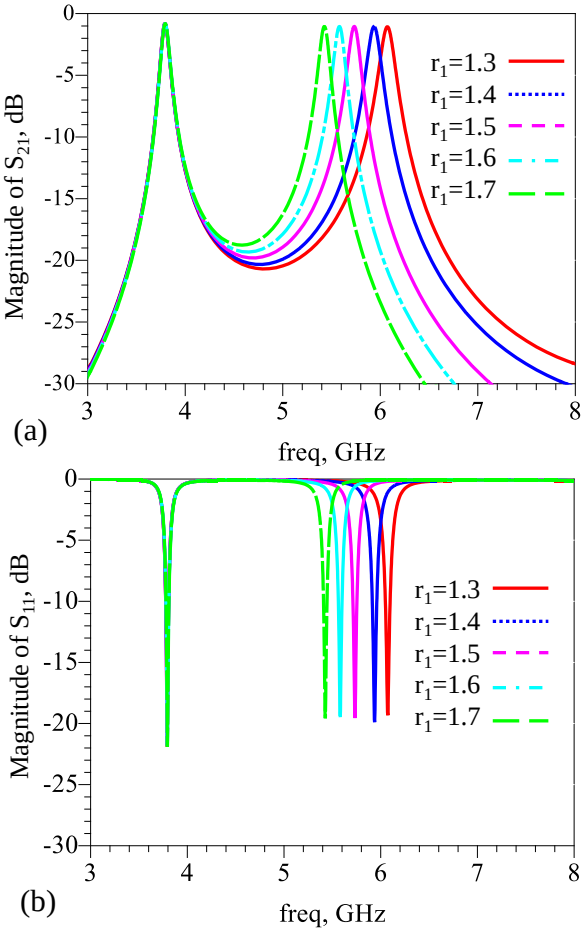

Fig. 8. Frequency response of the proposed dual-band BP filter for different values of r_1 (a) S_{21}, (b) S_{11}.

V. INVESTIGATION OF THE SURFACE CURRENT DENSITY OF THE PROPOSED FILTER

In this section, to clarify the operating mechanism of the dual-band BP filter, the surface current densities of two passbands (3.7 and 5.7 GHz) are investigated. Fig. 9 shows this scenario. As seen, the current between the input and output ports of the BPF exists for two passbands. Also, Fig. 9 (a) (the surface current density of the first passband) shows that a large surface current density is induced on the U-shaped waveguide. In the other passband frequency (Fig. 9 (b)), the current distributions become more concentrated at the bottom section of the disk resonator and the stub resonator.

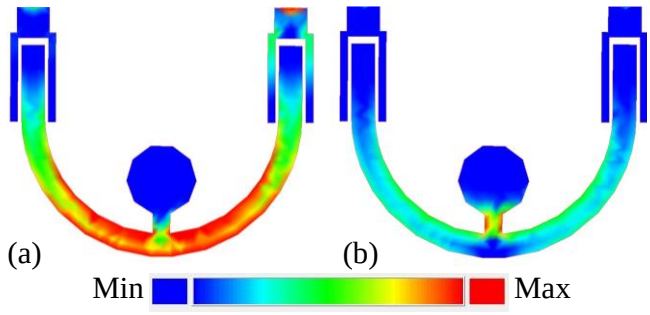

Fig. 9. The current density distribution of the proposed dual-band BP filter at (a) 3.7 GHz, and (b) 5.7 GHz.

VI. RESULTS AND COMPARISONS

The proposed dual-band BP filter is designed on Rogers_RO4003 substrate (h= 20 mil, ε_r= 3.38, and loss tangent= 0.0022) and simulated by the method of moments in ADS software. The proposed filter has two passbands centering at 3.7 and 5.7 GHz with maximum insertion losses of 0.62 and 0.75 dB, and return losses better than 21.9 and 20.1 dB. Moreover, the maximum attenuation level in the stopbands (before the first band, between two bands, and after the second band) is more than 20 dB. The circuit size of the proposed filter is 12.55 × 9.9 mm^2. It is worth mentioning that its second band can be tuned by changing the radius of the disk resonator without the necessity to change the total circuit size.

Finally, to create a better view of the reliability of the obtained results, the main parameters of the proposed filter are compared to other works in Table I. These parameters are the resonance frequencies (f_r), insertion losses (IL), and return losses (RL) of the resonance frequencies, the upper stop-band bandwidths, and the total sizes of the filters. Each of these compared parameters is further discussed.

According to the table, BP filters can have one or several passbands. Here, BP filters with one, two, and three passbands are investigated. In an ideal filter, to pass signals in the passbands without any weakening, the insertion loss values of the passbands should be low and the return loss values of the passbands have to be high in the passbands. For the proposed filter designed in this paper, the desirable values for insertion loss and return loss are less than 1 dB and more than 20 dB, respectively. As observed, the suggested BP filter is among the lowest insertion loss and highest return loss filters.

The other compared parameter is the upper stop-band bandwidth based on the highest resonance frequency ratio. As seen, the proposed filter falls within the highest stop-band bandwidth. The last parameter that is investigated is the total sizes of the filters. As known, having a compact size is one of the advantages that should be considered in the design of microwave devices. Therefore, in this paper, by considering such a property, the proposed filter is well-designed. In addition to the desirable properties mentioned in Table 1, the proposed filter has other advantages. For example, its simple and symmetrical structure resulted in no distinction between the input and output ports. Furthermore, its second resonance frequency can be easily tuned without increasing the overall size. On the whole, the proposed BP filter has several advantageous features compared to the other relevant designs.

TABLE I
Performance Comparisons Among the Proposed Dual-Band Bp Filter and Other Relevant Designs

Ref	f_r (GHz)	IL (dB)	RL (dB)	Stop-band Bandwidth	Size (mm^2)
[70]	1.8 3.7 5.5	2.23 2.98 3.31	17.2 33.6 17.9	0.63 f_{r3}	35×22
[71]	1.5 2.4	1.1 0.9	21.2 21.2	1.16 f_{r2}	25×15.3
[72]	2.55 3.65	1.22 2.13	20 20	0.098 f_{r2}	41.2×41.5
[73]	2.4 3.6	1.2 1.67	12 12	0.48 f_{r2}	17.5×17.5
[74]	2.4 5.8	1.28 0.96	18.2 21.8	0.086 f_{r2}	1.7×3.6
[75]	2.45 5.43	1.8 1.4	16 16	0.055 f_{r2}	16×17.2
[76]	5.2 8.04	0.8 0.8	14 14	0.9 f_{r2}	22.2×11.9
[77]	2.7 3.65	0.8 0.8	>21 >21	0.83 f_{r2}	11.1×8
[78]	2.1 2.6	0.68 1.08	19.3 30.7	1.4 f_{r2}	16.4×13.4
[79]	2	0.8	>25	0.37 f_{r2}	40×14.38
This work	3.7 5.7	0.62 0.75	21.9 20.1	0.75 f_{r2}	12.9×9.5

VII. CONCLUSION

In Summary, the optimal characteristics of a novel compact dual-band BP filter using a microstrip structure are presented in this paper. The proposed filter structure is composed of a disk resonator coupled to a U-shaped waveguide through a stub resonator. Utilization of a U-shaped waveguide contributes to shrinking the size of the structure. Also, using a disk resonator creates the property of tunability in the second band. Moreover, there is no distinction between the input and output ports due to the symmetrical structure of the filter. With all these suitable features, the proposed filter is applicable for Wi-MAX and WLAN Systems applications.

ACKNOWLEDGMENT

The author acknowledges Semnan University for supporting the team throughout the research. Also, the author would like to thank the editor and reviewers for their constructive comments.

REFERENCES

[1] Hong, J. S. G., & Lancaster, M. J., Microstrip filters for RF/microwave applications, 2004, John Wiley & Sons.

[2] Ebadi, S. M., & Khani, S. (2023). Highly-Miniaturized Nano-Plasmonic Filters Based on Stepped Impedance Resonators with Tunable Cut-Off Wavelengths. Plasmonics, 1-12.

[3] Hamouleh-Alipour, A., Khani, S., Ashoorirad, M., & Baghbani, R. (2023). Trapped multimodal resonance in magnetic field enhancement and sensitive THz plasmon sensor for toxic materials accusation. IEEE Sensors Journal, 23 (13), 14057-14066.

[4] Korani, N., Abbasi, A., & Danaie, M. (2023). Band-pass and band-stop plasmonic filters based on Wilkinson power divider structure. Plasmonics, 1-10.

[5] Khani, S., & Hayati, M. (2022). Optical biosensors using plasmonic and photonic crystal band-gap structures for the detection of basal cell cancer. Scientific reports, 12(1), 5246.

[6] Korani, N., Hajshahvaladi, L., & Danaie, M. (2024). Realization of a single-mode plasmonic bandpass filter based on a ring-shaped resonator and silver nanorods. Optical and Quantum Electronics, 56(1), 23.

[7] Khani, S., Danaie, M., & Rezaei, P. (2018). Realization of single-mode plasmonic bandpass filters using improved nanodisk resonators. Optics Communications, 420, 147-156.

[8] Khani, S., & Hayati, M. (2022). Optical sensing in single-mode filters based on surface plasmon H-shaped cavities. Optics Communications, 505, 127534.

[9] Moazami, A., Hashemi, M., & Shirazi, N. C. (2019). High efficiency tunable graphene-based plasmonic filter in the THz frequency range. Plasmonics, 14(2), 359-363.

[10] Khani, S., Danaie, M., & Rezaei, P. (2019). Tunable single-mode bandpass filter based on metal–insulator–metal plasmonic coupled U-shaped cavities. IET Optoelectronics, 13(4), 161-171.

[11] Zhou, L., Tan, Y., Ji, D., Zhu, B., Zhang, P., Xu, J., ... & Zhu, J. (2016). Self-assembly of highly efficient, broadband plasmonic absorbers for solar steam generation. Science advances, 2(4), e1501227.

[12] Huang, Z., Li, S., Cui, X., Wan, Y., Xiao, Y., Tian, S., ... & Lee, C. S. (2020). A broadband aggregation-independent plasmonic absorber for highly efficient solar steam generation. Journal of Materials Chemistry A, 8(21), 10742-10746.

[13] Ebadi, S. M., & Khani, S. (2023). Design of a tetra-band MIM plasmonic absorber based on triangular arrays in an ultra-compact MIM waveguide. Optical and quantum electronics, 55(6), 482.

[14] Ye, Y., Xie, Y., Song, T., Wang, Y., Chai, J., Liu, B., & Liu, Y. (2019). Design of a novel plasmonic splitter with variable transmissions and selectable channels. IEEE Transactions on Nanotechnology, 18, 617-625.

[15] Gao, X., Zhou, L., Yu, X. Y., Cao, W. P., Li, H. O., Ma, H. F., & Cui, T. J. (2015). Ultra-wideband surface plasmonic Y-splitter. Optics Express, 23(18), 23270-23277.

[16] Chang, K. W., & Huang, C. C. (2016). Ultrashort broadband polarization beam splitter based on a combined hybrid plasmonic waveguide. Scientific reports, 6(1), 19609.

[17] Khani, S., & Afsahi, M. (2023). Optical refractive index sensors based on plasmon-induced transparency phenomenon in a plasmonic waveguide coupled to stub and nano-disk resonators. Plasmonics, 18(1), 255-270.

[18] Duan, Q., Liu, Y., Chang, S., Chen, H., & Chen, J. H. (2021). Surface plasmonic sensors: Sensing mechanism and recent applications. Sensors, 21(16), 5262.

[19] Khani, S., & Hayati, M. (2021). An ultra-high sensitive plasmonic refractive index sensor using an elliptical resonator and MIM waveguide. Superlattices and Microstructures, 156, 106970.

[20] Ooi, K. J., Chu, H. S., Bai, P., & Ang, L. K. (2014). Electro-optical graphene plasmonic logic gates. Optics letters, 39(6), 1629-1632.

[21] Yang, X., Hu, X., Yang, H., & Gong, Q. (2017). Ultracompact all-optical logic gates based on nonlinear plasmonic nanocavities. Nanophotonics, 6(1), 365-376.

[22] Al-Musawi, H. K., Al-Janabi, A. K., Al-abassi, S. A., Abusiba, N. A. H. A., & Al-Fatlawi, N. A. H. Q. (2020). Plasmonic logic gates based on dielectric-metal-dielectric design with two optical communication bands. Optik, 223, 165416.

[23] Khani, S., Danaie, M., & Rezaei, P. (2021). Fano Resonance using surface plasmon polaritons in a nano-disk resonator coupled to perpendicular waveguides for amplitude modulation applications. Plasmonics, 16(6), 1891-1908.

[24] Ayata, M., Fedoryshyn, Y., Heni, W., Baeuerle, B., Josten, A., Zahner, M., ... & Leuthold, J. (2017). High-speed plasmonic modulator in a single metal layer. Science, 358(6363), 630-632.

[25] Khani, S., Danaie, M., & Rezaei, P. (2022). Plasmonic all-optical modulator based on the coupling of a surface Plasmon stub filter and a meandered MIM waveguide. Optical and Quantum Electronics, 54(12), 849.

[26] Chen, J., Li, Z., Zhang, X., Xiao, J., & Gong, Q. (2013). Submicron bidirectional all-optical plasmonic switches. Scientific reports, 3(1), 1451.

[27] Wu, H. Y., Huang, Y. T., Shen, P. T., Lee, H., Oketani, R., Yonemaru, Y., ... & Chu, S. W. (2016). Ultrasmall all-optical plasmonic switch and its application to superresolution imaging. Scientific reports, 6(1), 24293.

[28] Khani, S., Farmani, A., & Rezaei, P. (2023). Optical resistance switch for optical sensing. In Artificial Intelligence in Mechatronics and Civil Engineering: Bridging the Gap (pp. 1-38). Singapore: Springer Nature Singapore.

[29] Bergthold, M., Wasserman, D., & Muhowski, A. J. (2022). Plasmon-enhanced distributed Bragg reflectors. Infrared Physics & Technology, 125, 104236.

[30] Wang, S., Hu, H., Liu, X., & Ding, T. (2023). Non-dispersive Fano resonances in hybrid plasmonic-distributed Bragg reflector structures. Nanophotonics, 12(16), 3211-3216.

[31] Khani, S., Farmani, A., & Mir, A. (2021). Reconfigurable and scalable 2, 4-and 6-channel plasmonics demultiplexer utilizing symmetrical rectangular resonators containing silver nano-rod defects with FDTD method. Scientific Reports, 11(1), 13628.

[32] Azar, M. T. H., Zavvari, M., Arashmehr, A., Zehforoosh, Y., & Mohammadi, P. (2017). Design of a high-performance metal–insulator–metal plasmonic demultiplexer. Journal of Nanophotonics, 11(2), 026002-026002.

[33] Khani, S., Danaie, M., & Rezaei, P. (2018). Double and triple-wavelength plasmonic demultiplexers based on improved circular nanodisk resonators. Optical Engineering, 57(10), 107102-107102.

[34] Navaei, M., & Rezaei, P. (2024). Permittivity measurement of fluidics with high sensitivity by chandelier form microwave sensor. Microwave and Optical Technology Letters, 66(1), e33955.

[35] Khani, S., & Hayati, M. (2017). Compact microstrip lowpass filter with wide stopband and sharp roll-off. Microw J, 60(11), 86-92.

[36] Sharbati, V., Rezaei, P., & Fakharian, M. M. (2016). A planar UWB antenna with switchable single/double band-rejection characteristics. Radioengineering, 25(3), 429-435.

[37] Khani, S., Danaie, M., & Rezaei, P. (2019). Miniaturized microstrip dual-band bandpass filter with wide upper stop-band bandwidth. Analog Integrated Circuits and Signal Processing, 98, 367-376.

[38] Fakharian, M. M., & Rezaei, P. (2014). Very compact palmate leaf-shaped CPW-FED monopole antenna for UWB applications. Microwave and Optical Technology Letters, 56(7), 1612-1616.

[39] Sharbati, V., Rezaei, P., & Fakharian, M. M. (2017). Compact planar UWB antenna with enhanced bandwidth and switchable band-notch function for WLAN and DSRC. IETE journal of research, 63(6), 805-812.

[40] Khani, S., Danaie, M., Rezaei, P., & Shahzadi, A. (2020). Compact ultra-wide upper stopband microstrip dual-band BPF using tapered and octagonal loop resonators. Frequenz, 74(1-2), 61-71.

[41] Najafi, M., & Hazeri, A. R. (2021). Microstrip dual-narrowband bandpass filter with independent passbands. Wireless Personal Communications, 119, 3503-3516.

[42] Moitra, S., & Dey, R. (2020). Design of dual-band and Tri-band Bandpass Filter (BPF) with Improved inter-band isolation using DGS integrated coupled microstrip lines structures. Wireless Personal Communications, 110(4), 2019-2030.

[43] Rekha, T. K., Abdulla, P., Jasmine, P. M., & Anu, A. R. (2020). Compact microstrip lowpass filter with high harmonics suppression using defected structures. AEU-International Journal of Electronics and Communications, 115, 153032.

[44] Yamanaka, K., Ishii, M., Akasegawa, A., Nakanishi, T., Baniecki, J. D., & Kurihara, K. (2008). 5 GHz HTS power filters with TM-mode microstrip-disk resonators. Physica C: Superconductivity, 468(15-20), 1950-1953.

[45] Yang, Q., Liu, S., Shi, H., Xu, K. D., Dai, X., Du, H., & Zhang, A. (2021). Design of Wideband Bandpass Filter Based on Corrugated Disk Resonator with Multiple Resonant Modes. Materials, 14(10), 2614.

[46] Bhat, Z. A., Sheikh, J. A., Khan, S. D., Rehman, R., & Ashraf, S. (2021). Compact and novel coupled line microstrip bandpass filter based on stepped impedance resonators for millimeter-wave communications. Frequenz, 75(5-6), 147-152.

[47] Tang, S. C., Chu, P. C., Kuo, J. T., Wu, L. K., & Lin, C. H. (2022). Compact microstrip wideband cross-coupled inline bandpass filters with miniaturized stepped-impedance resonators (SIRs). IEEE Access, 10, 21328-21335.

[48] Navaei, M., Rezaei, P., & Kiani, S. (2022). Microwave split ring resonator sensor for determination of the fluids permittivity with measurement of human milk samples. Radio Science, 57(7), 1-11.

[49] Pandey, P., Pandey, A. K., & Chauhan, R. K. (2022). Novel Tri-band Microstrip Bandpass Filter with Stub Loaded in Circular Ring Resonator. In VLSI, Microwave and Wireless Technologies: Select Proceedings of ICVMWT 2021 (pp. 357-366). Singapore: Springer Nature Singapore.

[50] Vineetha, K. V., Kumar, M. S., & Madhav, B. T. P. (2021, February). Analysis of Triple Band Split Ring Resonator Based Microstrip Bandpass Filter. In Journal of Physics: Conference Series (Vol. 1804, No. 1, p. 012149). IOP Publishing.

[51] Song, K., Zhu, Y., Zhao, M., Fan, M., & Fan, Y. (2017). Miniaturized bandpass filter using dual-mode hexagonal loop resonator. International Journal of Microwave and Wireless Technologies, 9(5), 1003-1008.

[52] Stefanovski Pajović, S. L., Potrebić, M. M., Tošić, D. V., & Cvetković, Z. Ž. (2016). Fabrication parameters affecting the implementation of waveguide bandpass filter with complementary split-ring resonators. Journal of Computational Electronics, 15, 1462-1472.

[53] Khani, S., Makki, S. V. A. D., Mousavi, S. M. H., Danaie, M., & Rezaei, P. (2017). Adjustable compact dual-band microstrip bandpass filter using T-shaped resonators. Microwave and Optical Technology Letters, 59(12), 2970-2975.

[54] Ogbodo, E., Wang, Y., & Yeo, K. S. (2016). Microstrip dual-band bandpass filter using U-shaped resonators. Progress In Electromagnetics Research Letters, 59, 1-6.

[55] Khani, S., Mousavi, S. M. H., Danaie, M., & Rezaei, P. (2018). Tunable compact microstrip dual-band bandpass filter with tapered resonators. Microwave and Optical Technology Letters, 60(5), 1256-1261.

[56] Karami, F., Rezaei, P., Amn-e-Elahi, A., Mousavirazi, Z., Denidni, T. A., & Kishk, A. A. (2020). A compact high-performance patch array with suppressed cross polarization using image feed.

[57] Razi, Z. M., & Rezaei, P. (2020). A two-layer beam-steering array antenna with 4× 4 modified Butler matrix fed network for switched beam application. International Journal of RF and Microwave Computer-Aided Engineering, 30(2), e22028.

[58] Siahkamari, H., Yasoubi, Z., Jahanbakhshi, M., Mousavi, S. M. H., Siahkamari, P., Nouri, M. E., ... & Azadi, R. (2018). Design of compact Wilkinson power divider with harmonic suppression using T-shaped resonators. Frequenz, 72(5-6), 253-259.

[59] Mohammad Hadi Mousavi, S., Salar Rahimi, M., Malakooti, S. A., Afzali, B., & Singh Virdee, B. (2016). A broadband out-of-phase gysel power divider based on a dual-band circuit with a single fixed isolation resistor. International Journal of RF and Microwave Computer-Aided Engineering, 26(9), 796-802.

[60] Roshani, S., Yahya, S. I., Mezaal, Y. S., Chaudhary, M. A., Al-Hilali, A. A., Mojirleilani, A., & Roshani, S. (2023). Design of a compact quad-channel microstrip diplexer for L and S-band applications. Micromachines, 14(3), 553.

[61] Lu, Q. Y., Zhang, Y. J., Cai, J., Qin, W., & Chen, J. X. (2020). Microstrip tunable diplexer with separately designable channels. IEEE Transactions on Circuits and Systems II: Express Briefs, 67(12), 2983-2987.

[62] Varcheh, H. N., Rezaei, P., & Kiani, S. (2023). A modified Jerusalem microstrip filter and its complementary for low phase noise X-band oscillator. International Journal of Microwave and Wireless Technologies, 15(10), 1707-1716.

[63] Bayati, M. S., Mousavi, S. M. H., & Makki, S. V. A. D. (2022). Combination of absorptive notch filter and tunable dual-band conventional notch filter. Microwave and Optical Technology Letters, 64(1), 30-35.

[64] Badamchi, B., Valizade, A., Rezaei, P., & Badamchi, Z. (2014). A reconfigurable square slot antenna with a switchable single band, UWB, and UWB with band notch function performances. Applied Computational Electromagnetics Society Journal, 29(5), 383.

[65] Ebadi, S. M., Khani, S., & Örtegren, J. (2024). Design of miniaturized wide band-pass plasmonic filters in MIM waveguides with tailored spectral filtering. Optical and Quantum Electronics, 56(5), 1-24.

[66] Danaie, M., Khani, S., Noorozzadeh, E., & Vahdani, M. (2019). Improving the performance of cadmium telluride solar cell (CdTe) with different buffer layers. Iranian Journal of Physics Research, 19(1), 139-147.

[67] Sun, S., Shi, J., Zhu, L., Rustagi, S. C., Kang, K., & Mouthaan, K. (2007). 40 GHz compact TFMS meander-line bandpass filter on silicon substrate. Electronics Letters, 43(25), 1433-1434.

[68] Hinojosa, J., Martínez-Viviente, F. L., & Alvarez-Melcon, A. (2021). Compact double-notch coplanar and microstrip bandstop filters using metamaterial—inspired open ring resonators. Electronics, 10(3), 330.

[69] Ye, Y., Wu, Y., Chen, J., Su, G., Wang, J., & Liu, J. (2023). Intelligent Design of Hairpin Filters Based on Artificial Neural Network and Proximal Policy Optimization. Applied Sciences, 13(16), 9379.

[70] Chomtong, P., & Akkaraekthalin, P. (2014). A triple-band bandpass filter using tri-section step-impedance and capacitively loaded step-impedance resonators for GSM, WiMAX, and WLAN systems. Frequenz, 68(5-6), 227-234.

[71] Lin, L., Sun, S. J., Wu, B., & Liang, C. H. (2014). Dual-band bandpass filter with wide upper stopband using quad-mode stepped impedance stub-loaded resonator. Electronics Letters, 50(16), 1145-1146.

[72] Ieu, W., Zhang, D., & Zhou, D. (2017). High-selectivity dual-mode dual-band microstrip bandpass filter with multi-transmission zeros. Electronics Letters, 53(7), 482-484.

[73] Duan, Q., Song, K., Chen, F., & Fan, Y. (2015). Compact dual-band bandpass filter using simply hybrid structures. Electronics Letters, 51(16), 1265-1266.

[74] Danaeian, M., Zarezadeh, E., & Ghayoumi-Zadeh, H. (2018). A compact and high-performance dual-band bandpass filter based on unbalanced composite right/left-handed transmission lines for WLANs applications. Analog Integrated Circuits and Signal Processing, 94, 469-479.

[75] Avinash, K. G., & Srinivasa Rao, I. (2017). Compact dual-band bandpass filter based on the dual-mode modified star-shaped resonator. Microwave and Optical Technology Letters, 59(3), 505-511.

[76] Mohammadi, B., Valizade, A., Nourinia, J., & Rezaei, P. (2015). Design of a compact dual-band-notch ultra-wideband bandpass filter based on wave cancellation method. IET Microwaves, Antennas & Propagation, 9(1), 1-9.

[77] Mousavi, S. M. H., Makki, S. V. A., Alirezaee, S., & Malakooti, S. A. (2019). Design of a narrow dual-band BPF with an independently tunable passband. Electronics Letters, 55(9), 542-543.

[78] Ghaderi, A., Golestanifar, A., & Shama, F. (2017). Design of a compact microstrip tunable dual-band bandpass filter. AEU-International Journal of Electronics and Communications, 82, 391-396.

[79] Huang, F., Wang, J., & Zhu, L. (2016). A new approach to design a microstrip dual-mode balun bandpass filter. IEEE Microwave and Wireless Components Letters, 26(4), 252-254.